HAL
open science

Investigating the effect of diagenesis on ESR dating of Middle Stone Age tooth samples from the open-air site of Lovedale, Free State, South Africa

Maïlys Richard, Edwige Pons-Branchu, Raanan Carmieli, Ifat Kaplan-Ashiri, Ana Alvaro Gallo, Giulia Ricci, Luisa Caneve, Kristen Wroth, Arnaud Dapoigny, Chantal Tribolo, et al.

To cite this version:

Maïlys Richard, Edwige Pons-Branchu, Raanan Carmieli, Ifat Kaplan-Ashiri, Ana Alvaro Gallo, et al.. Investigating the effect of diagenesis on ESR dating of Middle Stone Age tooth samples from the open-air site of Lovedale, Free State, South Africa. Quaternary Geochronology, 2022, 69, pp.101269. 10.1016/j.quageo.2022.101269 . hal-03607523

HAL Id: hal-03607523

https://hal.science/hal-03607523v1

Submitted on 5 Jan 2023

HAL is a multi-disciplinary open access archive for the deposit and dissemination of scientific research documents, whether they are published or not. The documents may come from teaching and research institutions in France or abroad, or from public or private research centers.

L'archive ouverte pluridisciplinaire **HAL**, est destinée au dépôt et à la diffusion de documents scientifiques de niveau recherche, publiés ou non, émanant des établissements d'enseignement et de recherche français ou étrangers, des laboratoires publics ou privés.

Investigating the effect of diagenesis on ESR dating of Middle Stone Age tooth samples from the open-air site of Lovedale, Free State, South Africa

Maïlys Richard [a,b,c,d,*], Edwige Pons-Branchu [b], Raanan Carmieli [e], Ifat Kaplan-Ashiri [e], Ana Alvaro Gallo [a], Giulia Ricci [f], Luisa Caneve [g], Kristen Wroth [h], Arnaud Dapoigny [b], Chantal Tribolo [i], Elisabetta Boaretto [j], Michael B. Toffolo [i]

[a] Centro Nacional de Investigací on sobre la Evolucí on Humana (CENIEH), 09002, Burgos, Spain
[b] Laboratoire des Sciences du Climat et de l'Environnement (LSCE), GEOTRAC-LSCE/IPSL, UMR 8212, CEA-CNRS-UVSQ, Universit´e Paris-Saclay, 91191, Gif-sur-Yvette, France
[c] Department of Early Prehistory and Quaternary Ecology, University of Tübingen, 72070, Tübingen, Germany
[d] Centre de Recherche Français a` J´erusalem (CRFJ), USR 3132, 9100401, Jerusalem, Israel
[e] Department of Chemical Research Support, Weizmann Institute of Science, 7610001, Rehovot, Israel
[f] Department of Geosciences, University of Padova, 35131, Padova, Italy
[g] ENEA, 00044, Frascati, Italy
[h] Institut für Naturwissenschaftliche Archa¨ologie, University of Tübingen, 72070, Tübingen, Germany
[i] Arch´eosciences Bordeaux, UMR 6034 CNRS-Universit´e Bordeaux Montaigne, 33607, Pessac, France
[j] Scientific Archaeology Unit, Weizmann Institute of Science, 7610001, Rehovot, Israel

ARTICLE INFO

Keywords:
Electron spin resonance
Uranium-series
Diagenesis
Infrared spectroscopy
Raman micro-spectroscopy
Cathodoluminescence
Laser-induced fluorescence
Micromorphology

ABSTRACT

Teeth are usually targeted for dating archaeological sites because they are less prone to dissolution, in comparison with bones. However, despite this apparent resistance, teeth do undergo diagenesis, which needs to be accounted for in order to obtain accurate ages. In particular, the uptake of trace elements such as uranium in dental tissues needs to be considered for dose rate determination when dated using electron spin resonance (ESR). Characterising the mineralogy and structural integrity of samples prior to dating may thus provide important information related to their state of preservation, especially in the case of teeth whose U content can significantly affect the dose rate.

In this study, we dated five teeth of small-sized bovids using combined ESR/U-series dating. They were collected at the Middle Stone Age site of Lovedale, located in the central interior of South Africa. Micromorphology provided sedimentary context to the samples, which were recovered from a layer of gravel rich in faunal remains. Using cathodoluminescence, laser-induced fluorescence, Fourier transform infrared spectroscopy and Raman micro-spectroscopy we assessed the degree of preservation of the enamel. Results reveal that carbonate hydroxyapatite underwent post-depositional alteration, based on its molecular structure and elemental compo- sition. Although the teeth all originate from the same layer and were sampled in the same 1-m square and at a similar elevation, U-content in the enamel differs highly from one tooth to the other, with values ranging from
1.7 to 29.6 ppm. These values are correlated with equivalent doses (D_e) from 228 to 923 Gy and are consistent with variations in crystallinity determined with vibrational spectroscopy. We also investigated the possible saturation of the ESR signal, by repeating measurements with microwave power values from 1 to 20 mW.

Despite such diversity in U-content, the ages calculated assuming an early uptake of U all fall within the same range, from 63 ± 8 ka to 68 ± 15 ka and may only represent a minimum estimate.

1. Introduction

Since the pioneering work of Ikeya and Miki (1980), fossil tooth enamel has been extensively used for electron spin resonance (ESR) to date prehistoric occupations. Compared to bones, teeth are made up of much larger crystals arranged in structures that are more resistant to

* Corresponding author. Centro Nacional de Investigacio´n sobre la Evolucio´n Humana (CENIEH), 09002, Burgos, Spain
E-mail address: mailys.richard@cenieh.es (M. Richard).

https://doi.org/10.1016/j.quageo.2022.101269
Received 30 November 2021; Received in revised form 20 February 2022; Accepted 4 March 2022
Available online 11 March 2022
1871-1014/© 2022 Elsevier B.V. All rights reserved.

chemical weathering (Weiner, 2010). Due to their apparent good pres- ervation in archaeological settings, they are a choice material for geochemical analyses (Lee-Thorp, 2008) and dating (Ikeya, 1993). However, diagenetic alteration processes have been reported in car- bonate hydroxyapatite [$Ca_{10}(PO_4,CO_3)_6(OH)_2$], the mineral component of teeth (e.g., Dauphin et al., 2018), which may affect both equivalent dose and dose rate. To control the quality of samples and ensure that they preserve unaltered signals, sample characterisation has proven to be useful in the field of stable isotopes geochemistry (e.g., Lee-Thorp and Sponheimer, 2003; Thomas et al., 2011; Rey et al., 2021). Indeed, changes in carbonate content and crystallinity, processes such as dissolution and recrystallisation, the presence of secondary phases, and the uptake of trace elements may affect the composition of bones and teeth (e.g., Hedges and Millard, 1995; Hedges, 2002; Trueman et al., 2004; Lebon et al., 2010; Dal Sasso et al., 2018a), and potentially the age determination. To date, the effect of such processes in relation to trapped-charge dating has been poorly investigated (Michel et al., 1995; Rink and Schwarcz, 1995) as opposed to the field of stable isotopes and trace elements analysis (e.g., Kohn et al., 1999; Sponheimer and Lee-Thorp, 1999; Schoeninger et al., 2003; Zazzo, 2014; Kamenov et al., 2018). In addition, it is well known that the uptake of uranium in dental tissues may significantly influence the dose rate (leading to the combi- nation of ESR with U-series; Grün et al., 1988), and that its distribution is heterogeneous (Eggins et al., 2003; Grün et al., 2008; Duval et al., 2011). It thus appears crucial to evaluate the effect of diagenesis on the sample and the impact on age determination, and to develop pre-screening methods to select the best-preserved samples. In this study, several characterisation techniques were used to track fossil tooth diagenesis, including Fourier transform infrared spectroscopy (FTIR), Raman micro-spectroscopy, scanning electron microscopy coupled with cath- odoluminescence (SEM-CL), and laser-induced fluorescence (LIF).

FTIR spectroscopy probes the vibrational modes of molecules, providing information about the chemical composition and structure of the material (Diem, 2015). FTIR in transmission mode can be used to assess the degree of atomic order (or 'crystallinity') of carbonate hy- droxyapatite crystals, which is related to their formation path (Termine and Posner, 1966). This process can be monitored by measuring the infrared splitting factor (IRSF) of the ν_4 absorption of phosphates, with higher values indicating increased crystallinity (Weiner and Bar-Yosef, 1990). However, it has been shown that two phenomena contribute to infrared absorptions in opposite ways. Pristine carbonate hydroxyapa- tite crystals are poorly ordered, which translates into broad infrared absorptions. At the same time, pristine crystals are small, causing peak narrowing. To decouple these two effects, Asscher et al. (2011b) developed a method whereby the IRSF is plotted against the full width at half maximum (FWHM) of the ν_3 absorption of phosphate over a number of grindings of the same KBr pellet, each time ground with increasing strength to reduce particle size. By doing so, it is possible to define trendlines (or 'grinding curves') that are characteristic for different types of carbonate hydroxyapatite (bone, enamel, dentine, cement) in different species. Upon ripening, pristine carbonate hydroxyapatite crystals become larger and more ordered at the atomic level, and this produces an offset in the grinding curves that can be used to identify diagenesis in faunal material (Asscher et al., 2011a).

Raman micro-spectroscopy, like FTIR, probes molecular vibrations (Diem, 2015). This technique has been applied to the study of bone diagenesis to detect collagen and carbonate content, the occurrence of secondary phases and the degree of crystallinity (e.g., Thomas et al., 2007; Lebon et al., 2011; Dal Sasso et al., 2018a). Broadening of the ν_1 absorption of carbonate hydroxyapatite is due to a decrease in atomic order (Penel et al., 1998; Puc´eat et al., 2004).

CL is the emission of light resulting from the excitation of electrons using an electron beam in a scanning electron microscope (SEM). Elec- trons in the valence band can be temporarily upgraded to an excited state following the irradiation by high-energy electrons. These electrons may be trapped in lattice defects during the relaxation to the ground

state, which are called 'luminescence centres'. When emptying the traps (relaxation to the ground state), light is emitted in the visible, NIR and UV range and the wavelength is characteristic of a chemical species (Boggs and Krinsley, 2006). SEM-CL can provide information regarding the incorporation of foreign ions in the enamel structure and their dis- tribution. For instance, it has been shown that rare earth elements (REE) and Mn are incorporated in bones and teeth during burial (e.g., Williams et al., 1997; Kohn et al., 1999); these are luminescence activators that can be detected using SEM-CL (S´egalen et al., 2008).

LIF uses a laser beam to excite electrons and produce electronic transitions. While relaxing to the ground state, fluorescence is emitted in the UV and visible ranges. As for CL, the wavelength of the emission is related to a specific chemical species. Only a few studies addressed the application of the technique to palaeontological specimens (Croft et al., 2004; Kaye et al., 2015) despite providing sensitive, non-destructive qualitative analyses using a remote and portable instrument. The fluo- rescence in minerals is sensitive to activator elements, impurity ions, defects, chemical composition, and crystal lattice (Gaft et al., 1998, 2001), and allows detecting trace elements in minerals (Bozlee et al., 2005; MacRae and Wilson, 2008).

We present here the ESR/U-series age results obtained for the base of the sequence of the Middle Stone Age (MSA) site of Lovedale, located in the central interior of South Africa, taking into consideration the effect of diagenetic alterations on the age results, and discussing the potential of integrating characterisation techniques to the dating process to ensure accurate age determinations.

2. Site description

Lovedale is an open-air site located on the left bank of the Modder River, in the Petrusburg District of western Free State, ~45 km SW of Florisbad (28°54.2′35″S; 25°41′7.69″E; 1220 m a.s.l.) (Fig. 1a). The Modder is a meandering river that flows westwards through the Free State 'panfield', a region characterised by many seasonally dry lakes (pans), which are interpreted as the remnant of an ancient paleo-drainage disrupted by tectonic activity (Grobler et al., 1988; Marshall and Harmse, 1992; Barker, 2011). River incision of the valley fill created a succession of alluvial terraces of different ages including a variety of channel and overbank deposits (Tooth et al., 2013). This region is located in the Highveld and it features an open, semi-arid grassland that belongs to the Grassland Biome, and which receives 450–530 mm of annual precipitation concentrated in the spring and summer (October to March) (Mucina and Rutherford, 2006). Rainfall often occurs in the form of thunderstorms, which promote surface run-off and thus erosion. This process, combined with river incision, results in the formation of erosional gullies ('dongas') in river terraces and the exposure of locales rich in lithic artefacts and/or fossils (Churchill et al., 2000; Brink et al., 2016; Bousman et al., in press). Lovedale is located in a relatively small donga, close to the top of an isolated crest that preserves an almost complete stratigraphic sequence of the river terrace (Fig. 1b).

Archaeological excavations led by M. Toffolo in 2019 and 2021 un- covered a MSA human occupation (Fig. 1c) dated to ~77-56 ka by optically stimulated luminescence (OSL) (Wroth et al., accepted). The large number of projectile points recovered during excavation and sur- face collection, together with cores and waste products of lithic reduc- tion, indicates that the site was a hunting preparation station. The combination of sediment micromorphology and FTIR spectroscopy showed that the stratigraphic sequence was deposited in 7 sedimentary units (SU) by low-energy water typical of overbank environments (Fig. 1e and f). A thin layer of aeolian sand (SU7) capping the sequence occurs discontinuously in the donga. All of the SUs underwent different degrees and types of post-depositional processes, including erosion, bioturbation, and pedogenesis. Phytolith analysis revealed that temperate climate conditions dominated throughout the sequence, except for early Marine Isotope Stage (MIS) 4, which was characterised by a dry spell (Wroth et al., accepted). About 10 m to the north of the main excavation trench, at the same elevation of basal SU1 but not in direct stratigraphic relation, a thin bed of fluvial gravel (Unit 9, Fig. 1d), consistent with a point-bar deposit, produced faunal remains of herbi- vores belonging to the Florisian Land Mammal Age (Brink, 1987, 2016), now called Late Naivashan (Van Couvering and Delson, 2020). FTIR analysis showed that many of the bones are diagenetically altered, as suggested by the cemented gravel found on their outer surface, whereas tooth enamel appears to be better preserved based on the degree of atomic order of carbonate hydroxyapatite (Wroth et al., accepted). The teeth analysed in this study were collected from this context in 2019.

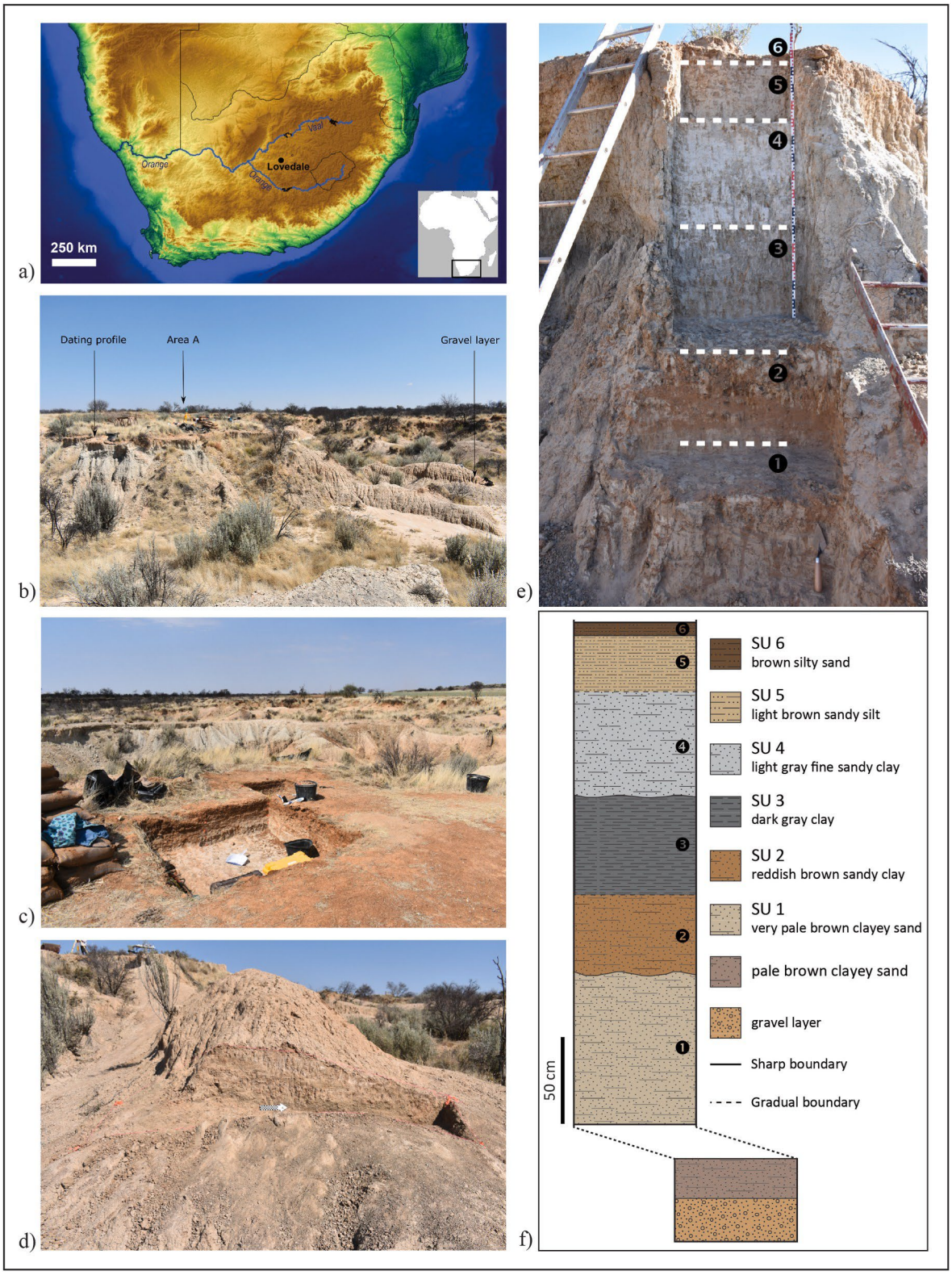

Fig. 1. Location of Lovedale in southern Africa (a), general view of the site and different studied areas (b), the excavated Area A (c), the gravel layer (d), the dating profile (e), and a schematic depiction of the sedimentary units (f). The map is modified from Toffolo et al. (2017).

3. Materials and methods

Five fragmentary teeth of small-sized bovids (LOV1180, 1197, 1200, 1201, and 1205), for which identification to species level was not possible, were collected from the gravel layer. They all come from the same 1 × 1 m square (SOM Figs. S1 and S2). They were collected with embedding sediment for the calculation of the beta dose rate. Two modern teeth were prepared for reference for the characterisation study: one from a lamb ('LAM', *Ovis aries*) and one from a springbok ('SPR', *Antidorcas marsupialis*). The latter is the closest to the extinct Florisian species of small-sized bovid, *Antidorcas bondi* (Brink, 1987, 2016; Brink and Lee-Thorp, 1992). Samples were prepared according to the pro- cedure of Richard et al. (2015), and more detailed information on the experimental protocol for ESR and U-series analyses is given in the SOM. In order to determine the effect of the microwave power value used for the stimulation, we also investigated the possible saturation of the ESR signal, by repeating measurements on sample LOV1180 with values of the microwave of 1, 2, 5, 10, 15, and 20 mW. Ages were calculated with 1σ error range using the DATA programme (Grün, 2009) that takes into account an alpha efficiency of 0.13 ± 0.02 (Grün and Katzenberger-Apel, 1994) and Monte-Carlo beta attenuation factors from Brennan et al. (1997). A water content (weight %) of 15 ± 5% for the sediment, of 0% for the enamel, and of 7 ± 5% for the dentine were assumed for the age calculation. The dose rate from the dental tissues was calculated assuming equilibrium in the U-series decay chain.

Two intact blocks of sediment (LOV21-1 and LOV21-2) were collected for micromorphological analysis from the exposed profile with clear interbedding of coarse-grained and fine-grained layers and where bones and teeth had been recovered in the 2019 field season. The description of the sediment is based on established protocols (Macphail and Goldberg, 2017; Stoops et al., 2018; Stoops, 2021).

With regard to characterisation analyses, details on the experimental protocols are given in the SOM. FTIR analyses were conducted on all samples, including the two modern analogues, lamb ('LAM') and springbok ('SPR') teeth, to obtain reference spectra. The IRSF of the ν_4 absorption, which is the sum of the peaks at 604 and 567 cm^{-1} divided by the height of the valley between them (Weiner and Bar-Yosef, 1990), was plotted against the FWMH of the ν_3 absorption at 1035 cm^{-1}, following the grinding curve method of Asscher et al. (2011a; 2011b) (Fig. 2). Raman analyses were conducted on 10 different points for each sample. We focused our attention on the most intense peak in the spectrum (961 cm^{-1}), corresponding to the symmetric stretching vi- bration of the PO_4^{3-} group. SEM-CL was employed to study several enamel aliquots of LOV1180 that were exposed to increasing amounts of radiation (0, 40, 90, 240, and 610 Gy). The data was collected in Spectrum Imaging (SI) mode, where simultaneous SEM image and spectra were collected for a defined region of interest (ROI); that way both the spectral information and electron image could be correlated. LIF measurements were performed on ~2 mg of powdered enamel from the five samples from Lovedale: both natural and irradiated aliquots (highest dose) were analysed. For comparison, a fossil enamel with low U-content (<10 ppb, powder form) from the Middle Palaeolithic site of Hohle Fels (HF2976) and the modern lamb enamel ('LAM') were measured, the latter both in fragment and powder form, in order to have a reference material free of uranium.

4. Results and discussion

4.1. Micromorphology

Three microfacies were described for the two samples: coarse gravel, fine gravel, and silty sand (see SOM for detailed description and Fig. S3). The coarse gravel facies is found only at the bottom of the sequence, but the fine gravel and silty sand are interbedded throughout the upper section of both samples. The sediments around Unit 9 appear to have been deposited via water with varying intensity. The coarse gravel is likely related to relatively fast-moving water at the edge of the riverbed, resulting in large grains (up to 4 mm) of very rounded bedrock and other material and very little fine sediment except in small pockets and rounded aggregates. This is the microfacies where faunal material was found. The finer gravel was likely deposited by slightly lower energy water flow, with a mix of rounded and sub-angular grains and more silt- sized fine fraction. Finally, the silty sand is the result of low-energy water movement, such as an overbank deposit.

The thin beds or lenses of fine sand that grade into silt at the top of this layer may have formed as puddles or pools of standing water dried out, forming a crust that dried and cracked on top. Some of these crusts can also be seen macroscopically in the section. The interbedded nature of these packets of fine gravel and silty sand indicates different flow regimes of the river, and the occurrence of intact beds and lenses con- firms that teeth were not displaced after deposition. There is also evi- dence for post-depositional groundwater movement based on the presence of iron and manganese staining, impregnations, coatings around void spaces, and rare small nodules found throughout the sam- ples, which was likely facilitated by the porous nature of gravel and promoted the diagenetic alteration of faunal material.

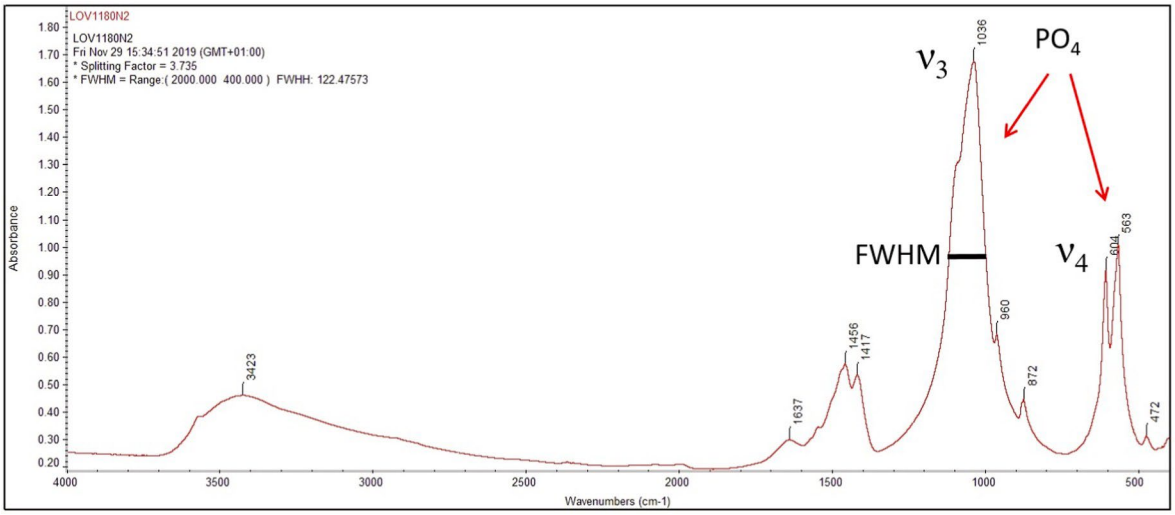

Fig. 2. FTIR spectrum of a natural enamel aliquot from Lovedale (LOV1180).

4.2. Electron spin resonance/U-series dating

Microwave saturation tests were conducted using values of 1, 2, 5, 10, 15, and 20 mW on LOV1180. ESR intensity increases as a function of the microwave power and the saturation curve suggests a saturation for values higher than 2 mW (SOM Figs. S4 and S5). However, the D_e calculated for each value of the microwave power used for the measurements all fall within the same range: 268 ± 57 Gy (1 mW), 274 ± 61 Gy (2 mW), 283 ± 71 Gy (5 mW), 273 ± 63 Gy (10 mW), 279 ± 63 Gy (15 mW), and 283 ± 70 Gy (20 mW) (SOM Fig. S6). Despite a high error on the D_e (likely due to the extrapolation from only five experimental points and to r^2 ranging from 0.986 (5 mW) to 0.989 (1 mW)), these data suggest that the value of the microwave power does not significantly affect the D_e.

All equivalent doses used for the age calculation were obtained using a value of 1 mW for the microwave power. They are presented in Table 1, together with the dose rate and age results. The D_e range from 268 ± 57 (LOV1180) to 923 ± 88 Gy (LOV1200). The fitting parameters and examples of dose response curves are provided in SOM (Table S1 and Fig. S7). Surprisingly, the D_e values are highly variable from one sample to the other. They can reach 449 ± 61 Gy (LOV1197) and 923 ± 88 Gy (LOV1200), although the teeth were collected in the same 1 × 1 m square in the gravel layer. Interestingly, the U-content in the enamel is abnormally high for these two samples (SOM Table S2), of 9.68 ± 0.08 (LOV1197) and 29.56 ± 0.26 (LOV 1200), providing internal dose rates of 3866 ± 394 and 11060 ± 1080 $\mu Gy \cdot a^{-1}$, respectively. On the con- trary, the environmental dose rate is homogeneous, ranging from 1176 to 1266 $\mu Gy \cdot a^{-1}$. The gamma dose rate measured *in situ* is 848 ± 20 $\mu Gy \cdot a^{-1}$ and the beta dose rate calculated using U, Th, and K content (see results in SOM Table S3) ranges from 166 ± 18 to 268 ± 28 $\mu Gy \cdot a^{-1}$. The dose rate from the dental tissues thus constitutes the main contri- bution to the dose rate.

U-content in the enamel is rarely higher than 2 ppm in Pleistocene open-air sites in the Modder River basin (e.g., Grün et al., 1996; Brink et al., 2016). The U-content is always higher in the dentine due to difference in composition. Here, the U-content is high and homogeneous from one dentine to the other, and ranges from 95.44 ± 0.79 to 143.07 ± 1.17 ppm (SOM Table S2). To check if contamination from the dentine could have led to overestimation of the U-content in the enamel and the D_e, a dentine aliquot of LOV1200 (14.4 mg, ~105 ppm of U) was measured using ESR spectrometry with the same experimental settings as for the enamel (~30 ppm of U). After subtracting the background and normalising by the aliquot mass, results indicate that the ESR intensity for the dentine aliquot represents 5% of the intensity of the natural enamel aliquot (see Fig. S8 for a comparison of the natural signal of the enamel and the dentin aliquots). This suggests that even if a small amount of dentine contaminated the enamel, the contribution to the ESR intensity and the D_e would be negligible. Moreover, for the five teeth, the U-content is positively correlated with the D_e values (Fig. 3) and all the ESR ages (calculated assuming early uptake, EU, see below) fall within the same range, thus excluding the possibility of contamination from the dentine, which would have led to biased U-content in the enamel. Isotopic ratios were measured to model the U uptake and to derive the dose rate (SOM Table S2). $^{234}U/^{238}U$ are homogeneous within the samples and are all higher than two. $^{230}Th/^{234}U$ range from 0.4926 ± 0.0010 to 0.7579 ± 0.0065 and the two samples with the higher U-content, of ~9.7 (LOV1197) and ~29.6 ppm (LOV1200), also have the highest $^{230}Th/^{234}U$ ratios. $^{230}Th/^{232}Th$ range from 99.9 ± 0.2 to 1627.8 ± 13.6 in the enamel and from 1495.8 ± 6.2 to 14325.0 ± 150.3 in the dentine, indicating that the contribution of detrital Th is negligible. Moreover, $^{232}Th/^{238}U$ content ratios are low, with values ranging from 0.0003 to 0.0366, which remain far from clay (or bulk earth) signature ca. 3–4 (Turekian and Wedepohl, 1961).

Apparent U-series ages (assuming no U or Th mobilisation) are older than 69 ka for all samples and are slightly older than the ESR ages (calculated assuming an early uptake), ranging from 68 ± 15 to 63 ± 4 ka (Table 1 and Fig. 3). For this reason, the ESR/U-series model proposed by Grün et al. (1988) to assess the U-uptake history of the dental tissues cannot be applied here, because U leaching may have occurred, the equivalent doses may be underestimated or some contributions of the dose rate may be overestimated. Considering that optically stimu- lated luminescence (OSL) dates of quartz samples are ~77-56 ka for the upper levels (Wroth et al., accepted) and that the ESR age calculation is limited to the use of the early uptake model, the ages presented here may be considered as minimum estimates.

4.3. Vibrational spectroscopy

The FWHM and IRSF of carbonate hydroxyapatite in all samples are presented in SOM Table S4 and the grinding curves in Fig. 4. The modern lamb and springbok produced overlapping trendlines, indicating that they exhibit similar degrees of atomic order, although one should keep in mind that there might be differences in FTIR signature between ju- venile and adult sheep. Archaeological samples LOV1180, 1201, and 1205 overlap with the springbok curve, and therefore, are well pre- served. On the contrary, the trendlines of samples LOV1197 and 1200 show significant offsets, which can be interpreted as the result of diagenesis (Asscher et al., 2011a). Interestingly, there is a direct corre- lation with the high U-content of these latter two samples, ~9.7 ppm and ~29.6 ppm, respectively. For the first time, a correlation between the degree of atomic order and the U-content is observed in enamel samples, supporting the use of FTIR grinding curves as a rapid, pre-screening method prior to ESR dating. Dissolution and reprecipita- tion processes in enamel carbonate hydroxyapatite are responsible for the increase in IRSF and can result in the incorporation or leaching of uranium, depending on variations in groundwater chemistry over time. Therefore, archaeological samples of enamel that exhibit high IRSF values compared to an unaltered reference standard should not be pri- oritised for ESR/U-series dating, given the uncertainty related to the degree of uranium leaching.

The mean values of the FWHM and shift of the 961 cm^{-1} Raman peak for the archaeological and modern samples are listed in SOM Table S5. Modern samples show the highest FWHM values, a feature that is indicative of poor atomic order (Dal Sasso et al., 2018b). The lamb tooth produced significantly different results, suggesting that Raman may be able to probe differences in atomic order that are not visible in FTIR,

Table 1
ESR data: equivalent dose and dose rate obtained for the teeth samples. Ages were calculated assuming an early uptake of U (EU, Bischoff and Rosenbauer, 1981).

Sample	D_e (Gy)	Dose rate (µGy·a^{-1})					
		sediment (γ)[a] + cosmic	sediment (β)[b]	enamel (α+β)	dentine (β)	Total	Age (ka)
LOV 1180	268 ± 57	963 ± 24	237 ± 24	602 ± 72	2125 ± 156	3927 ± 175	68 ± 15
LOV 1197	449 ± 61	963 ± 24	213 ± 23	3866 ± 394	1793 ± 151	6835 ± 423	66 ± 10
LOV 1200	923 ± 88	963 ± 24	303 ± 29	11060 ± 1080	2358 ± 192	14684 ± 1098	63 ± 8
LOV 1201	288 ± 19	963 ± 24	166 ± 18	816 ± 96	2567 ± 195	4512 ± 219	64 ± 5
LOV 1205	228 ± 11	963 ± 24	268 ± 28	667 ± 80	1732 ± 131	3630 ± 158	63 ± 4

[a] The gamma dose rate of 848 ± 20 µGy·a^{-1} was measured *in situ*. For a depth of 4.6 ± 1 m, the cosmic dose rate is 115 ± 13 µGy·a^{-1}.
[b] The beta dose rate was derived from U, Th, and K content measured using HPGe-gamma spectrometry. Results are presented in SOM Table S3.

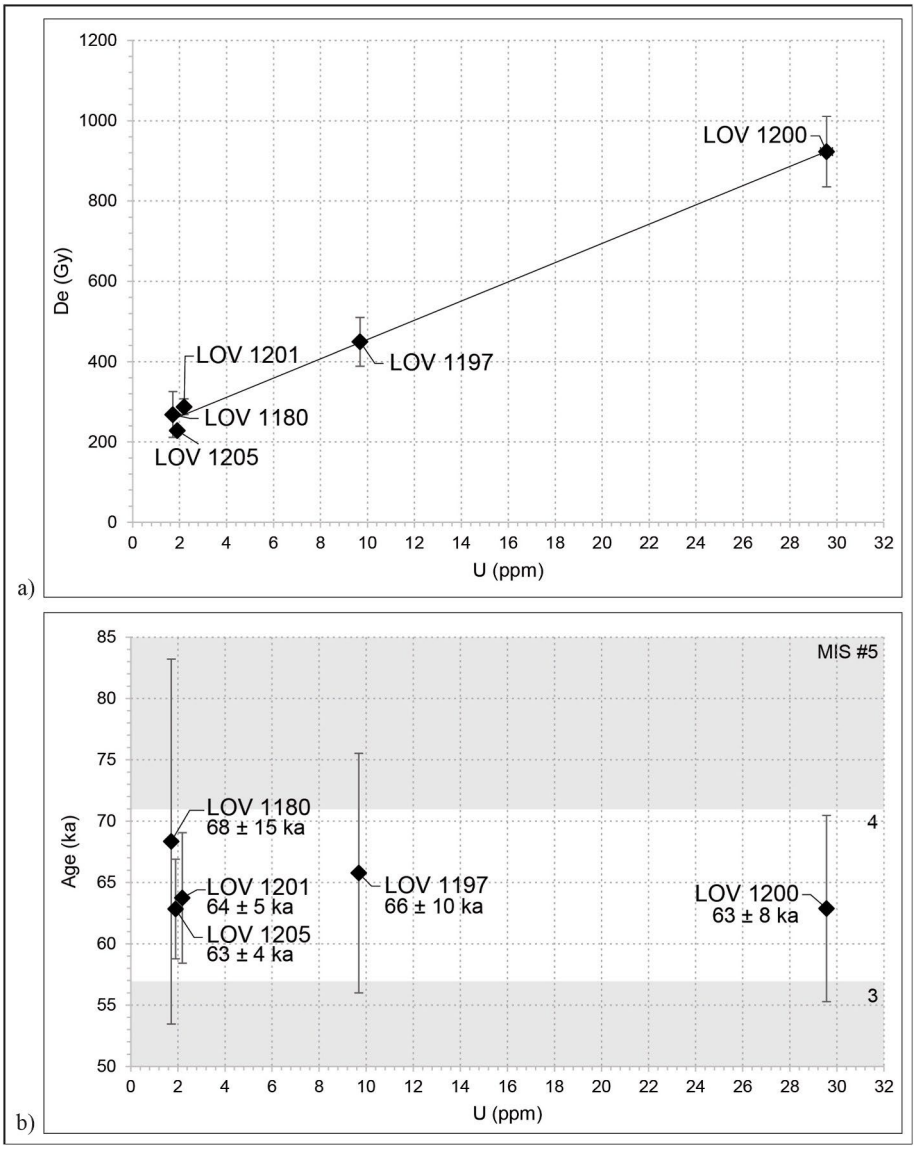

Fig. 3. Graphic representation of U-content in the enamel as a function of D_e (a) and ESR-EU ages (b).

although we should state once again that juvenile and adult sheep teeth might behave differently. All archaeological samples exhibit lower FWHM values, whereas the shift of the peak at 961 cm^{-1} does not vary significantly (Fig. 5). The sample with the highest U-content (LOV 1200, ~29.6 ppm) shows the highest value for the shift, but this trend does not appear for LOV1197 (~9.7 ppm), which is more similar to the springbok compared to other archaeological samples that contain less uranium. Contrary to FTIR results, the relationship between the degree of crys- tallinity and the U-content in the enamels does not clearly appear when using the FWHM and the shift of the peak at 961 cm^{-1}; nonetheless, it allows observing an increased crystallinity in the fossil samples.

4.4. Luminescence characterisation techniques

The SEM-CL results of the different aliquots of LOV1180 are presented in SOM Figs. S9, S10, S11 in the form of true colour maps and as spectra correlated to the SEM image. A synthesis of the results obtained from the 90 Gy aliquot is shown in Fig. 6.

The CL true colour maps in Fig. 6a and SOM Fig. S9 show a dominant purple-blue emission in all five samples. The spectra collected for each sample show a peak at ~450 nm (see Fig. 6f and SOM Fig. S10). This emission was observed in all hundreds of spectra acquired for each sample in all the regions that were measured, and it is considered an intrinsic luminescence (Blanc et al., 2000; S´egalen et al., 2008) related to the natural lattice defects of the carbonate hydroxyapatite crystal. The minor emission in the orange-red is caused by the presence of Mn^{2+} substituting for Ca^{2+}. The blue-purple colour of many pixels in the true colour map implies that the intrinsic emission band is the most intense band in the spectra, hence the dominant emission band of the samples. A closer look at the maps reveals rare pixels with a brown colour.

Several spectra that can be correlated with these pixels are presented in Fig. 6 and SOM Fig. S11. These spectra show emission bands at various wavelengths: 480, 570, 600, 650, 700, and 720 nm. The 600 nm emis- sion is related to the presence of Mn^{2+} in the Ca^{2+} sites of apatite and is known as a luminescence activator in this compound. Other peaks can be assigned to rare earth elements (REEs) such as Dy^{3+} (480 nm, 570 nm), Sm^{3+} (650 nm), Eu^{3+} (620 nm, 700 nm), and Sm^{2+} (720 nm). REEs can activate various luminescence bands with sharp emission peaks observed in the spectra in the range of 300–1000 nm (Blanc et al., 2000; S´egalen et al., 2008). These spectra were observed in all five samples with no correlation to the intensity of radiation. These elements were incorporated in the enamel as a consequence of the diagenesis (e.g., Trueman and Tuross, 2002: Fig. 7; Trueman et al., 2004) and can be used as tracers to assess the degree of preservation of the enamel.

No differences between irradiated and natural powder aliquots were observed with LIF, as is the case with SEM-CL results (SOM Fig. S12). The modern lamb enamel was analysed in both powder (P) and fragment

(F) forms that have different characteristic spectra, probably due to an inhomogeneous distribution of luminescence centres (SOM Fig. S13). This sample is characterised by six bands at ~310, 330, 390, 422, 442, and 472 nm (SOM Fig. S13). Generally, bands in the blue can be assigned to the intrinsic emissions of carbonate hydroxyapatite caused by lattice defects, whereas other bands are consistent with the occurrence of trace elements such as Mn2+ substituting for Ca2+ (Go¨tze et al., 2001). Furthermore, REEs (mainly Eu2+, Ce3+, Dy3+, Nd3+, and Sm3+) can also easily substitute for Ca2+ in the crystal lattice, and the charge compensation occurs by intrinsic electron defects, depletion of the constituent ions, and coupled substitution of the constituent ions by REE3+ (OH-, CO3OH3-, etc.) (Gaft et al., 1996, 2001; Habermann et al., 2000). Comparing our results with those reported in the literature, the modern enamel might be characterised by luminescence bands caused by intrinsic defects (310, 330 nm), Ce3+ substitution in Ca(I) and Ca(II) sites (390, 422, 442 nm), and Eu2+ substitution (472 nm) detected as a weak shoulder on the Ce3+ luminescence tail in the same luminescence spectral range of Ce3+ and Eu2+ (Gaft et al., 2001). However, due to the

complex crystallographic structure of hydroxyapatite, there might be other potential luminescence activators. Beside substitution in Ca(I), Ca (II), and P sites, Roman-Lopez et al. (2014) observed broad bands in natural bones and collagen around 440 and 490 nm that may be assigned to the tetrahedral anion $(PO_4)^{3+}$ or to structural defects.

The characteristic spectra obtained from the archaeological teeth are presented in Fig. 7. All samples present a broad band at around 460 nm or 485 nm, as opposed to the modern enamel spectra, which exhibit multiple peaks. The contribution of the UO^{2+} activator centre is determined based on the presence of multiple narrow peaks between 450 and 600 nm (Gaft et al., 1996; Reeder et al., 2000; Smith et al., 2015; Toffolo et al., 2019). These peaks are visible in the aragonite sample used for comparison. Sharp peaks are not visible in the archae- ological samples, and in the case of very small amounts of uranyl ions incorporated in the tooth, the broad bands at 460 and 485 nm cover the uranyl signal. However, the band at 485 nm is present in the spectra of the two samples LOV1197 and LOV1200, which contain 9.7 and 29.6 ppm of U, respectively, and exhibit high IRSF values. This shift to higher wavelengths may be due to the presence of uranyl in the crystal lattice in such high concentrations (>2 ppm).

These results show the potential of LIF in detecting the presence of large amounts of uranium in enamel carbonate hydroxyapatite as a result of diagenetic processes. The latter may include uranium leaching, and for this reason LIF may be used to select for ESR/U-series dating only the archaeological samples that do not contain significant amounts of uranyl. However, the analyses were performed on small powdered aliquots, which may reduce the quality of the luminescence acquisitions. For this reason, future analyses will be focused on acquiring spectra from tooth fragments.

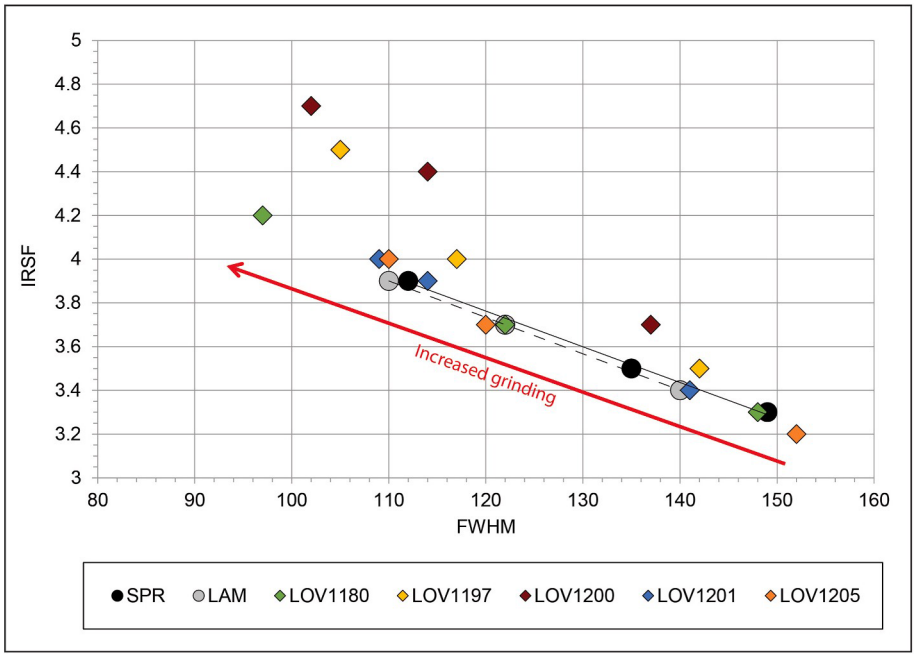

Fig. 4. Grinding curves constructed from the infrared splitting factor (IRSF) and the full width at half maximum (FWHM) calculated for the modern (SPR = springbok, solid line; LAM = lamb, dashed line) and fossil (LOV) samples from this study.

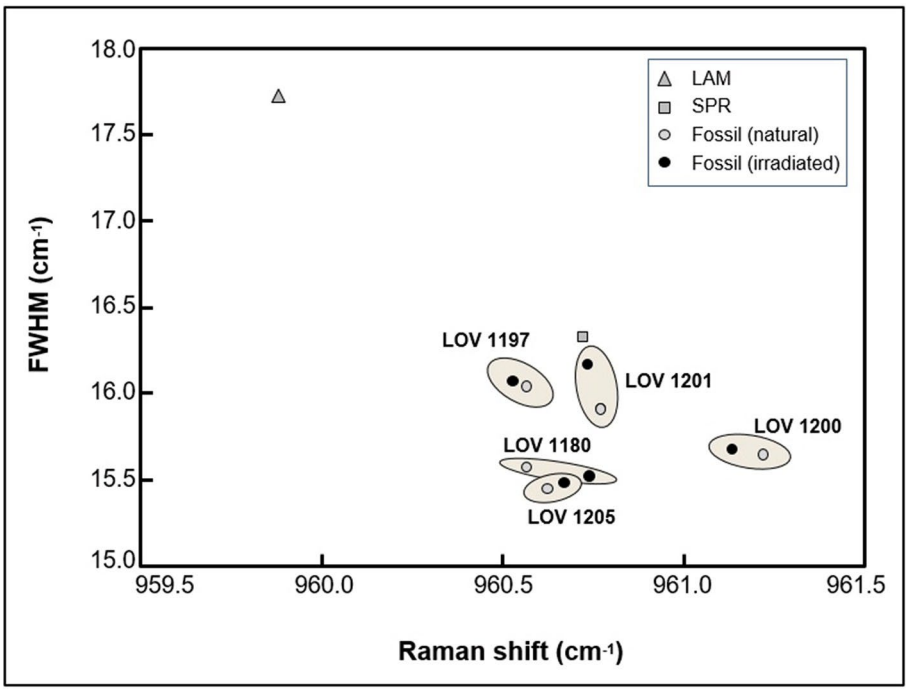

Fig. 5. FWHM and the frequency of the peak at 961 cm^{-1} obtained using Raman micro-spectroscopy on the modern (SPR = springbok; LAM = lamb) and fossil (LOV) samples.

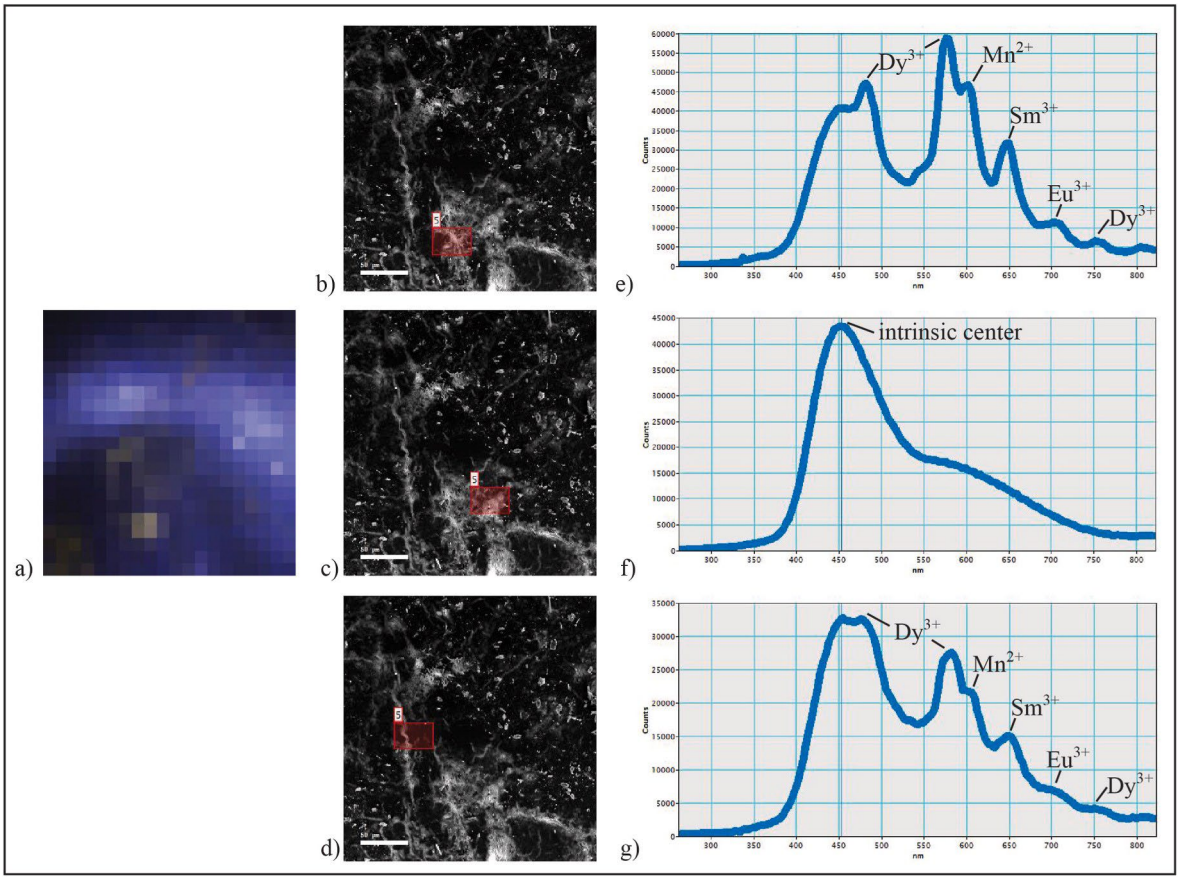

Fig. 6. SEM-CL results obtained on the LOV1180 aliquot irradiated at 90 Gy. a: colour map; b–d: SEM images; e–g: spectra showing the CL emission correlated to the SEM image.

5. Conclusions

This research, combining structural characterisation and ESR/U-series dating of modern and archaeological teeth, showed that the de- gree of diagenesis of the latter varies considerably, even though they were all collected within the same 1 m square and were not displaced after deposition. The range of uranium contents and crystallinity may be due to differential exposure to groundwater movement, as suggested by micromorphological analyses. It thus appears crucial to characterise the samples individually, as well as the sedimentary context, to be able to combine mineralogy with the age results and shed more light into the effects of diagenetic processes on ESR dating.

ESR and U-series data showed that the high U-content (>2 ppm) in some of the enamels is positively correlated with high D_e and does not seem to affect the age calculation using the EU model. Indeed, ages all fall within the same range, providing a weighted mean age of 64 ± 3 ka for the gravel layer. Moreover, the power of the microwave used for the ESR measurements of LOV1180, ranging from 1 to 20 mW, does not significantly affect the D_e values. Since the U-uptake modelling was limited to the use of the early uptake model, which provides a maximum dose rate from the dental tissue, the ESR ages presented here may be considered as minimum estimates, in agreement with the available OSL ages for the upper part of the sequence that range from ~77 to ~56 ka. Lovedale is thus one of the only two sites that date to the early MIS 4 in the Free State, and the only one in open air (Pienaar et al., 2008).

It is crucial to focus on well-preserved and in-situ teeth samples to apply ESR dating. Characterisation studies prior to dating may give useful insights into the preservation of dateable materials such as fossil teeth and will certainly help building reliable chronologies for the human evolution timeline.

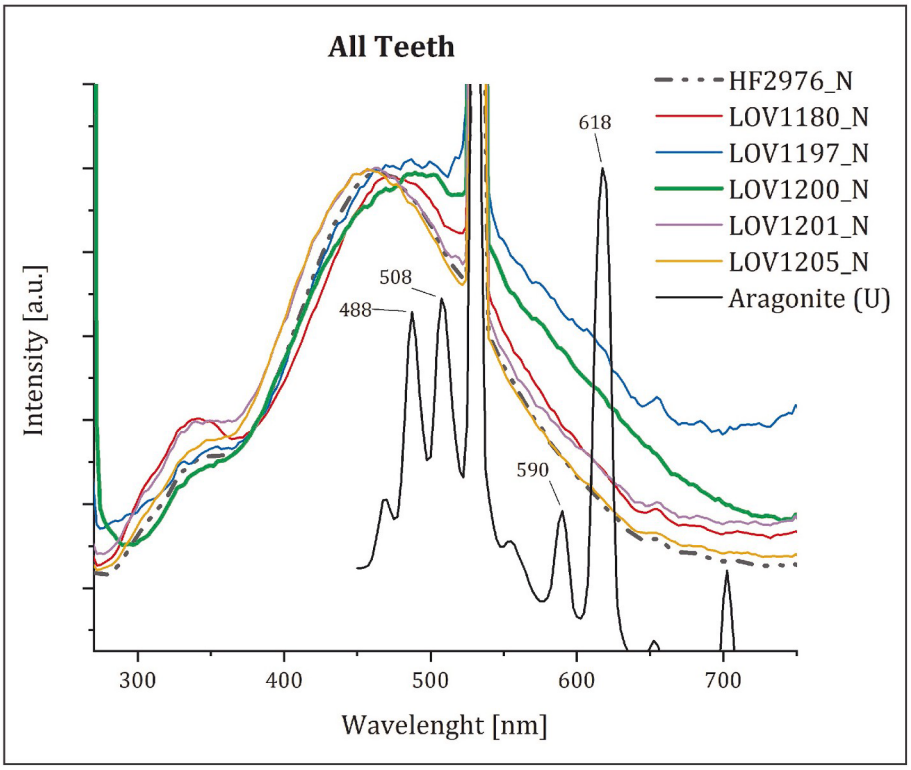

Fig. 7. Characteristic LIF spectra collected from the fossil teeth (N = natural aliquot), including the Lovedale samples and a low U-content enamel from Hohle Fels (HF, dashed line). A spectrum of aragonite containing U was obtained by the authors and used as reference (Toffolo et al., 2019).

Declaration of competing interest

The authors declare that they have no known competing financial interests or personal relationships that could have appeared to influence the work reported in this paper.

Acknowledgments

This study was part of two postdoctoral fellowships granted to M. Richard, from the French Research Institute in Jerusalem (2019, "international mobility fellowship") and from the University of Tübingen (2020, "Teach@Tübingen"). Part of the analyses was funded by a grant from the Deutsche Forschungsgemeinschaft (n. MI 1748/4-1) to C. E. Miller (University of Tübingen). M. Toffolo was funded by a grant from IdEx Bordeaux (grant n. ANR-10-IDEX-03-02). Archaeological excavations at Lovedale were conducted under the auspices of the National Museum Bloemfontein, with a permit from the South African Heritage Resources Agency (permit ID 2862 to L. Rossouw and M. Toffolo). We wish to thank F. Du Toit for allowing excavations at the Lovedale Farm,

L. Kolska Horwitz (Hebrew University of Jerusalem) for faunal identification, L. Rossouw (National Museum Bloemfontein) for providing the modern springbok tooth, I. Lombardi for Raman analyses, and L. Buchbinder (Technion) and M. J. Alonso (CENIEH) for sample irradiation. We thank the guest editor and the anonymous reviewer for their constructive comments on our manuscript.

Appendix A. Supplementary data

Supplementary data to this article can be found online at https://doi. org/10.1016/j.quageo.2022.101269.

References

Asscher, Y., Regev, L., Weiner, S., Boaretto, E., 2011a. Atomic disorder in fossil tooth and bone mineral: an FTIR study using the grinding curve method. Arch´eoSciences 35, 135–141.

Asscher, Y., Weiner, S., Boaretto, E., 2011b. Variations in atomic disorder in biogenic carbonate hydroxyapatite using the infrared spectrum grinding curve method. Adv. Funct. Mater. 21, 3308–3313.

Barker, C.H., 2011. Utilising published data for DTM construction and drainage basin delineation in the Modder River catchment, Free State, South Africa. S. Afr. Geogr. J. 93, 89–103.

Bischoff, J.L., Rosenbauer, R.J., 1981. Uranium series dating of human skeletal remains from the Del mar and Sunnyvale sites, California. Science 213, 1003–1005.

Blanc, P., Baumer, A., Cesbron, F., Ohnenstetter, D., Panczer, G., R´emond, G., 2000. Systematic cathodoluminescence spectral analysis of synthetic doped minerals: anhydrite, apatite, calcite, fluorite, Scheelite and zircon. In: Pagel, M., Barbin, V., Blanc, P., Ohnenstetter, D. (Eds.), Cathodoluminescence in Geosciences. Springer, pp. 127–160.

Boggs, S., Krinsley, D., 2006. Application of Cathodoluminescence Imaging to the Study of Sedimentary Rocks. Cambridge University Press, Cambridge.

Bousman, C.B., Brink, J.S., Rossouw, L., Bateman, M.D., Morris, S.E., Meier, H., Cohen, B., Trower, G., Herries, A.I.R., Palmison, M., Ringstaff, C., Thornton-Barnett, S., Dworkin, S., (in press). Erfkroon: late quaternary alluvial geology, paleoenvironments and Stone age archaeology in the western free state, South Africa, in: Beyin, A., Wright, D.K., Wilkins, J., Bouzouggar, A., Olszewski, D.I. (Eds.), Handbook of Pleistocene Archaeology of Africa: Hominin Behavior, Geography, and Chronology. Springer.

Bozlee, B.J., Misra, A.K., Sharma, S.K., Ingram, M., 2005. Remote Raman and fluorescence studies of mineral samples. Spectrochim. Acta Mol. Biomol. Spectrosc. 61, 2342–2348.

Brennan, B.J., Rink, W.J., McGuirl, E.L., Schwarcz, H.P., Prestwich, W.V., 1997. Beta doses in tooth enamel by "one-group" theory and the ROSY ESR dating software. Radiat. Meas. 27, 307–314.

Brink, J.S., 1987. The Archaeozoology of Florisbad, Orange Free State, vol. 24. Memoirs van die Nasionale Museum, Bloemfontein, pp. 1–151.

Brink, J.S., 2016. Faunal evidence for a mid- and late Quaternary environmental change in southern Africa. In: Knight, J., Grab, S.W. (Eds.), Quaternary Environmental Change in Southern Africa: Physical and Human Dimensions. Cambridge University Press, Cambridge.

Brink, J.S., Bousman, C.B., Grün, R., 2016. A reconstruction of the skull of *Megalotragus priscus* (Broom, 1909), based on a find from Erfkroon, Modder River, South Africa, with notes on the chronology and biogeography of the species. Palaeoecol. Afr. 33, 71–94.

Brink, J.S., Lee-Thorp, J.A., 1992. The feeding niche of an extinct springbok, *Antidorcas bondi* (Antelopini, Bovidae), and its palaeoenvironmental meaning. South Afr. J. Sci. 88, 227–229.

Churchill, S.E., Brink, J.S., Berger, L.R., Hutchinson, R.A., Rossouw, L., Stynder, D., Hancox, P.J., Brandt, D., Woodborne, S., Loock, J.C., Scott, L., Ungar, P., 2000. Erfkroon: a new Florisian fossil locality from fluvial contexts in the western Free State, South Africa. South Afr. J. Sci. 96, 161–163.

Croft, D.A., Kaye, T., Panko, L., 2004. A new method for finding small vertebrate fossils: ultraviolet light at night. Palaeontology 47, 795–800.

Dal Sasso, G., Angelini, I., Maritan, L., Artioli, G., 2018a. Raman hyperspectral imaging as an effective and highly informative tool to study the diagenetic alteration of fossil bones. Talanta 179, 167–176.

Dal Sasso, G., Asscher, Y., Angelini, I., Nodari, L., Artioli, G., 2018b. A universal curve of apatite crystallinity for the assessment of bone integrity and preservation. Sci. Rep. 8, 12025.

Dauphin, Y., Castillo-Michel, H., Denys, C., El Hajraoui, M.A., Nespoulet, R., Stoetzel, E., 2018. Diagenetic alterations of Meriones incisors (rodentia) of El Harhoura 2 cave, Morocco (late pleistocene–middle holocene). PalZ 92, 163–177.

Diem, M., 2015. Modern Vibrational Spectroscopy and Micro-spectroscopy: Theory, Instrumentation and Biomedical Applications. Wiley.

Duval, M., Aubert, M., Hellstrom, J., Grün, R., 2011. High resolution LA-ICP-MS mapping of U and Th isotopes in an early Pleistocene equid tooth from Fuente Nueva-3 (Orce, Andalusia, Spain). Quat. Geochronol. 6, 458–467.

Eggins, S., Grün, R., Pike, A.W.G., Shelley, M., Taylor, L., 2003. ^{238}U, ^{232}Th profiling and U-series isotope analysis of fossil teeth by laser ablation-ICPMS. Quat. Sci. Rev. 22, 1373–1382.

Gaft, M., Panczer, G., Reisfeld, R., Uspensky, E., 2001. Laser-induced time-resolved luminescence as a tool for rare-earth element identification in minerals. Phys. Chem. Miner. 28, 347–363.

Gaft, M., Reisfeld, R., Panczer, G., Blank, P., Boulon, G., 1998. Laser-induced time-resolved luminescence of minerals. Spectrochim. Acta Mol. Biomol. Spectrosc. 54, 2163–2175.

Gaft, M., Shoval, S., Panczer, G., Nathan, Y., Champagnon, B., Garapon, C., 1996. Luminescence of uranium and rare-earth elements in apatite of fossil fish teeth. Palaeogeogr. Palaeoclimatol. Palaeoecol. 126, 187–193.

Go¨tze, J., Heimann, R., Hildebrandt, H., Gburek, U., 2001. Microstructural investigation into calcium phosphate biomaterials by spatially resolved cathodoluminescence. Mater. Werkst. 32, 130–136.

Grobler, N.J., Loock, J.C., Behounek, N.J., 1988. Development of pans in paleodrainage in the north-western orange free state. Palaeoecol. Afr. Surround. Isl. 19, 87–96.

Grün, R., 2009. The DATA program for the calculation of ESR age estimates on tooth enamel. Quat. Geochronol. 4, 231–232.

Grün, R., Aubert, M., Joannes-Boyau, R., Moncel, M.-H., 2008. High resolution analysis of uranium and thorium concentration as well as U-series isotope distributions in a Neanderthal tooth from Payre (Ard`eche, France) using laser ablation ICP-MS. Geochem. Cosmochim. Acta 72, 5278–5290.

Grün, R., Brink, J.S., Spooner, N.A., Taylor, L., Stringer, C.B., Franciscus, R.G., Murray, A.S., 1996. Direct dating of Florisbad hominid. Nature 382, 500–501.

Grün, R., Katzenberger-Apel, O., 1994. An alpha irradiator for ESR dating. Ancient TL 12, 35–38.

Grün, R., Schwarcz, H.P., Chadam, J., 1988. ESR dating of tooth enamel: coupled correction for U-uptake and U-series disequilibrium. Int. J. Radiat. Appl. Instrum. Nucl. Tracks Radiat. Meas. 14, 237–241.

Habermann, D., Go¨tte, T., Meijer, J., Stephan, A., Richter, D., Niklas, J., 2000. High resolution rare-earth elements analyses of natural apatite and its application in geo-sciences: combined micro-PIXE, quantitative CL spectroscopy and electron spin resonance analyses. Nucl. Instrum. Methods Phys. Res. Sect. B Beam Interact. Mater. Atoms 161, 846–851.

Hedges, R.E.M., 2002. Bone diagenesis: an overview of processes. Archaeometry 44, 319–328.

Hedges, R.E.M., Millard, A.R., 1995. Bones and groundwater: towards the modelling of diagenetic processes. J. Archaeol. Sci. 22, 155–164.

Ikeya, M., 1993. New Applications of Electron Spin Resonance. World Scientific Publishing, Singapour, p. 500.

Ikeya, M., Miki, T., 1980. Electron Spin Resonance Dating of Animal and Human Bones. The American Association for the Advancement of Science, pp. 977–979.

Kamenov, G.D., Lofaro, E.M., Goad, G., Krigbaum, J., 2018. Trace elements in modern and archaeological human teeth: implications for human metal exposure and enamel diagenetic changes. J. Archaeol. Sci. 99, 27–34.

Kaye, T.G., Falk, A.R., Pittman, M., Sereno, P.C., Martin, L.D., Burnham, D.A., Gong, E., Xu, X., Wang, Y., 2015. Laser-stimulated fluorescence in paleontology. PLoS One 10, e0125923.

Kohn, M.J., Schoeninger, M.J., Barker, W.W., 1999. Altered states: effects of diagenesis on fossil tooth chemistry. Geochem. Cosmochim. Acta 63, 2737–2747.

Lebon, M., Müller, K., Bellot-Gurlet, L., Paris, C., Reiche, I., 2011. Application des micro-spectrom´etries infrarouge et Raman `a l´etude des processus diag´en´etiques alt´erant les ossements pal´eolithiques. ArcheoSci. Revue d'arch´eom´etrie 179–190.

Lebon, M., Reiche, I., Bahain, J.J., Chadefaux, C., Moigne, A.M., Fro¨hlich, F., S´emah, F., Schwarcz, H.P., Falgu`eres, C., 2010. New parameters for the characterization of diagenetic alterations and heat-induced changes of fossil bone mineral using Fourier transform infrared spectrometry. J. Archaeol. Sci. 37, 2265–2276.

Lee-Thorp, J., Sponheimer, M., 2003. Three case studies used to reassess the reliability of fossil bone and enamel isotope signals for paleodietary studies. J. Anthropol. Archaeol. 22, 208–216.

Lee-Thorp, J.A., 2008. On isotopes and old bones. Archaeometry 50, 925–950.

Macphail, R.I., Goldberg, P., 2017. Applied Soils and Micromorphology in Archaeology. Cambridge University Press, Cambridge.

MacRae, C.M., Wilson, N.C., 2008. Luminescence database I—minerals and materials. Microsc. Microanal. 14, 184–204.

Marshall, T.R., Harmse, J.T., 1992. A review of the origin and propagation of pans. South Afr. Geogr. 19, 9–21.

Michel, V., Ildefonse, P., Morin, G., 1995. Chemical and structural changes in *Cervus elaphus* tooth enamels during fossilization (Lazaret cave): a combined IR and XRD Rietveld analysis. Appl. Geochem. 10, 145–159.

Mucina, L., Rutherford, M.C., 2006. The Vegetation of South Africa, Lesotho and Swaziland. South African National Biodiversity Institute, Pretoria.

Penel, G., Leroy, G., Rey, C., Bres, E., 1998. MicroRaman spectral study of the PO_4 and CO_3 vibrational modes in synthetic and biological apatites. Calcif. Tissue Int. 63, 475–481.

Pienaar, M., Woodborne, S., Wadley, L., 2008. Optically stimulated luminescence dating at Rose Cottage cave. South Afr. J. Sci. 104, 65–70.

Puc´eat, E., Reynard, B., L´ecuyer, C., 2004. Can crystallinity be used to determine the degree of chemical alteration of biogenic apatites? Chem. Geol. 205, 83–97.

Reeder, R.J., Nugent, M., Lamble, G.M., Tait, C.D., Morris, D.E., 2000. Uranyl incorporation into calcite and aragonite: XAFS and luminescence studies. Environ. Sci. Technol. 34, 638–644.

Rey, L., Tacail, T., Santos, F., Rottier, S., Goude, G., Balter, V., 2021. Disentangling diagenetic and biogenic trace elements and Sr radiogenic isotopes in fossil dental enamel using laser ablation analysis. Chem. Geol. 120608.

Richard, M., Falgu`eres, C., Pons-Branchu, E., Bahain, J.J., Voinchet, P., Lebon, M., Valladas, H., Dolo, J.M., Puaud, S., Ru´e, M., Daujeard, C., Moncel, M.H., Raynal, J. P., 2015. Contribution of ESR/U-series dating to the chronology of late Middle Palaeolithic sites in the middle Rhoˆne valley, southeastern France. Quat. Geochronol. 30, 529–534.

Rink, W.J., Schwarcz, H.P., 1995. Tests for diagenesis in tooth enamel: ESR dating signals and carbonate contents. J. Archaeol. Sci. 22, 251–255.

Roman-Lopez, J., Correcher, V., Garcia-Guinea, J., Rivera, T., Lozano, I., 2014. Thermal and electron stimulated luminescence of natural bones, commercial hydroxyapatite and collagen. Spectrochim. Acta Mol. Biomol. Spectrosc. 120, 610–615.

Schoeninger, M.J., Hallin, K., Reeser, H., Valley, J.W., Fournelle, J., 2003. Isotopic alteration of mammalian tooth enamel. Int. J. Osteoarchaeol. 13, 11–19.

S´egalen, L., de Raf´elis, M., Lee-Thorp, J.A., Maurer, A.-F., Renard, M., 2008. Cathodoluminescence tools provide clues to depositional history in Miocene and Pliocene mammalian teeth. Palaeogeogr. Palaeoclimatol. Palaeoecol. 266, 246–253.

Smith, K.F., Bryan, N.D., Swinburne, A.N., Bots, P., Shaw, S., Natrajan, L.S., Mosselmans, J.F.W., Livens, F.R., Morris, K., 2015. U (VI) behaviour in hyperalkaline calcite systems. Geochem. Cosmochim. Acta 148, 343–359.

Sponheimer, M., Lee-Thorp, J.A., 1999. Alteration of enamel carbonate environments during fossilization. J. Archaeol. Sci. 26, 143–150.

Stoops, G., 2021. Guidelines for Analysis and Description of Soil and Regolith Thin Sections, second ed. Wiley.

Stoops, G., Marcelino, V., Mees, F., 2018. Interpretation of Micromorphological Features of Soils and Regoliths, second ed. Elsevier, Oxford.

Termine, J.D., Posner, A.S., 1966. Infrared analysis of rat bone: age dependency of amorphous and crystalline mineral fractions. Science 153, 1523–1525.

Thomas, D.B., Fordyce, R.E., Frew, R.D., Gordon, K.C., 2007. A rapid, non-destructive method of detecting diagenetic alteration in fossil bone using Raman spectroscopy.
J. Raman Spectrosc. 38, 1533–1537.

Thomas, D.B., McGoverin, C.M., Fordyce, R.E., Frew, R.D., Gordon, K.C., 2011. Raman spectroscopy of fossil bioapatite — a proxy for diagenetic alteration of the oxygen isotope composition. Palaeogeogr. Palaeoclimatol. Palaeoecol. 310, 62–70.

Toffolo, M.B., Brink, J.S., van Huyssteen, C., Berna, F., 2017. A microstratigraphic reevaluation of the Florisbad spring site, Free State Province, South Africa: formation processes and paleoenvironment. Geoarchaeology 32, 456–478.

Toffolo, M.B., Ricci, G., Caneve, L., Kaplan-Ashiri, I., 2019. Luminescence reveals variations in local structural order of calcium carbonate polymorphs formed by different mechanisms. Sci. Rep. 9, 16170.

Tooth, S., Hancox, J.P., Brandt, D., McCarthy, T.S., Jacobs, Z., Woodborne, S., 2013. Controls on the genesis, sedimentary architecture, and preservation potential of the dryland alluvial successions in stable continental interiors: insights from the incising Modder River, South Africa. J. Sediment. Res. 83, 541–561.

Trueman, C.N., Tuross, N., 2002. Trace elements in recent and fossil bone apatite. Rev. Mineral. Geochem. 48 (1), 489–521.

Trueman, C.N.G., Behrensmeyer, A.K., Tuross, N., Weiner, S., 2004. Mineralogical and compositional changes in bones exposed on soil surfaces in Amboseli National Park, Kenya: diagenetic mechanisms and the role of sediment pore fluids. J. Archaeol. Sci. 31, 721–739.

Turekian, K.K., Wedepohl, K.H., 1961. Distribution of the elements in some major units of the earth's crust. Geol. Soc. Am. Bull. 72, 175–192.

Van Couvering, J.A., Delson, E., 2020. African Land mammal ages. J. Vertebr. Paleontol. 40, e1803340.

Weiner, S., 2010. Microarchaeology. Beyond the Visible Archaeological Record. Cambridge University Press, New York.

Weiner, S., Bar-Yosef, O., 1990. States of preservation of bones from prehistoric sites in the near east: a survey. J. Archaeol. Sci. 17, 187–196.

Williams, C.T., Henderson, P., Marlow, C.A., Molleson, T.I., 1997. The environment of deposition indicated by the distribution of rare earth elements in fossil bones from Olduvai Gorge, Tanzania. Appl. Geochem. 12, 537–547.

Wroth, K., Tribolo, C., Bousman, C.B., Kolska Horwitz, L., Rossouw, L., Miller, C.E., Toffolo, M.B., accepted. Human occupation of the semi-arid grasslands of South Africa during MIS 4: new archaeological and paleoecological evidence from Lovedale, Free State. Quat. Sci. Rev..

Zazzo, A., 2014. Bone and enamel carbonate diagenesis: a radiocarbon perspective. Palaeogeogr. Palaeoclimatol. Palaeoecol. 416, 168–178.